Prediction of residual stress within linear friction welds using a computationally efficient modelling approach

Buhr, C, Ahmed, B, Colegrove, PA, McAndrew, AR, Guo, H & Zhang, X

Original citation:
Buhr, C, Ahmed, B, Colegrove, PA, McAndrew, AR, Guo, H & Zhang, X 2018, 'Prediction of residual stress within linear friction welds using a computationally efficient modelling approach' *Materials & Design*, vol 139, pp. 222-233
https://dx.doi.org/10.1016/j.matdes.2017.11.013

DOI 10.1016/j.matdes.2017.11.013
ISSN 0261-3069
ESSN 0264-1275

Publisher: Elsevier

Materials and Design 139 (2018) 222–233

Contents lists available at ScienceDirect

Materials and Design

journal homepage: www.elsevier.com/locate/matdes

Prediction of residual stress within linear friction welds using a computationally efficient modelling approach

Clément Bühr [a,*], Bilal Ahmad [b], Paul A. Colegrove [a], Anthony R. McAndrew [a], Hua Guo [b], Xiang Zhang [b]

[a] Cranfield University, Cranfield, Bedfordshire MK43 0AL, UK
[b] Coventry University, Coventry CV1 5FB, UK

HIGHLIGHTS

- The modelling approach predicts residual stresses within linear friction welds with notably reduced computational time.
- Increasing the rubbing velocity increased the peak residual stress and narrowed the band of tensile residual stress.
- The residual stress distribution is strongly affected by the thermal gradient of the equilibrium temperature field.
- High weld interface temperature enlarges the band of tensile residual stress.

GRAPHICAL ABSTRACT

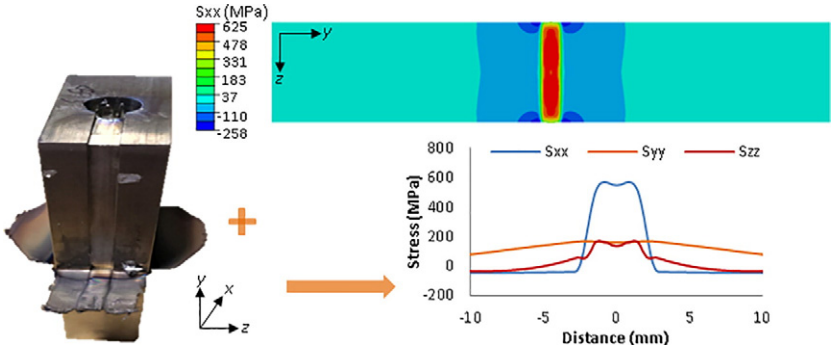

ARTICLE INFO

Article history:
Received 21 September 2017
Received in revised form 25 October 2017
Accepted 7 November 2017
Available online 8 November 2017

Keywords:
Linear friction welding
Titanium
Residual stress
Modelling
Experiments

ABSTRACT

Modelling the mechanical mixing occurring at the interface of a linear friction weld (LFW) is complex, making it difficult to study the development of residual stresses within real engineering workpieces. To address this, a sequentially-coupled numerical model of a Ti-6Al-4V LFW was developed, bypassing the modelling of the oscillations by applying the heat at the weld interface and sequentially removing rows of elements to account for the burn-off. Increasing the rubbing velocity was found to numerically increase the peak of residual stress while narrowing the distribution. Only small changes arose from increasing the applied pressure or changing the oscillation direction. Predictions suggested a strong correlation between the phase 3 temperature profile and the residual stress field subsequently created. Validation against neutron diffraction and contour method are also presented. This approach provides a computationally efficient technique to study the residual stress development within large 3D structures.

1. Introduction

Linear friction welding is a solid-state joining process which has been successfully implemented to manufacture titanium and nickel-based superalloy bladed-disks [1]. The process works by linearly rubbing one workpiece against another while applying a compressive force. Heat is generated first by friction then by plastic deformation. If appropriate parameters are used, the microstructure at the joint refines, resulting in higher hardness [2] and tensile strength [3] compared to the parent material. LFW is fast compared to other welding processes (typically under 10 s) and offers good repeatability [4].

LFW is typically divided into four phases: initial, transition, equilibrium and forging phases [5–9]. During the initial phase, heat is generated by friction of the asperities located at the interfaces of the workpieces. The transition phase begins once the temperature is sufficient to create

* Corresponding author.
E-mail address: c.buhr@cranfield.ac.uk (C. Bühr).

https://doi.org/10.1016/j.matdes.2017.11.013

a viscoplastic layer and material starts to be expelled, forming the flash. This is followed by the equilibrium phase, where a quasi-steady state is reached for the interface force, thermal profile and burn-off rate. Most of the flash is created during this phase and once the desired upset is reached, the motion is ceased rapidly, the workpieces are realigned and a forging force is applied to consolidate the joint.

Numerical modelling has been successfully used to gain knowledge of a wide range of outputs including temperature history [8,10–13], flash morphology [11,13], interface contaminants [12] and residual stress [14,15]. Unlike other friction welding processes, LFW numerical models are mostly fully-coupled [5–8,11–14,16–25]. There are two dominant approaches to account for the heat generated during the welding phases within a numerical model. The first method uses a temperature dependant friction coefficient [8,17,19,22–24] with a fully-coupled model to generate the heat during all the welding phases. Because several factors [26] can influence the friction coefficient (contact geometry, material properties, relative motion, applied forces, temperature, stiffness and vibrations), extra care is required when using friction coefficient values. The second method was first used by McAndrew et al. [6,12,21] and uses machine data recorded during welding which was post-processed to determine the average heat flux over the initial phase. This was applied to a thermal model to predict the temperature distribution. After this, the single-body method was used to model the equilibrium phase and an inelastic heat fraction was specified, typically in the range of 90 to 100% [5,12], to represent the amount of mechanical work converted to heat. The single-body method was originally developed by Turner et al. [5] and involves representing the two workpieces with a single body on which a thermal profile is mapped to account for the heat input from the initial phases. This approach allows the material at the centre to deform and realistic prediction of the flash morphology can be achieved [11,13]. Both of these approaches involve modelling the oscillations and as a result, large 3D models are computationally expensive and time consuming (between 4 and 6 weeks [21]). Therefore, models are often limited to two dimensions and complex geometries cannot be considered.

A limited number of publications on the numerical prediction of residual stress within Ti-6Al-4V LFW structures are available in the literature. Turner et al. [14] conducted a fully coupled thermo-mechanical analysis using the single-body modelling approach while applying a plane-strain condition to a 2D model. Oscillations of the equilibrium phase were simulated and inelastic heat produced within the deforming material was used to predict equilibrium temperature and stress fields before cooling the structure to atmospheric temperature and predicting the residual stress. A 3D model was not considered since it would have led to a prohibitively large computational time. Turner's FEA model replicated numerically the welding conditions investigated by Romero et al. [27] who conducted synchrotron X-ray diffraction experiments. Numerically, a larger band of residual stress was predicted compared to experiments. It is difficult to judge if the peak value was correctly predicted by the FEA model due to the lack of experimental data at the weld interface and its vicinity. Overall, there was a reasonable agreement between the experiments and simulations.

Nikiforov et al. [28] developed a numerical approach focused on the forging stage of the welding process. Nikiforov started his analysis by applying a forging pressure onto the 3D numerical model which was maintained at ambient temperature. A temperature field previously predicted using a 1D analytical model (constant thermal properties were used) was then mapped onto the model. Finally, while maintaining the temperature field, the forging pressure was removed before cooling down the part to ambient and predicting the residual stress field. Nikiforov experimentally calculated average values of residual stresses across the interface by measuring the interface dimensions before and after cutting the weld along its cross section. Estimations of the internal forces as a function of elastic material properties and weld cross section dimensions were used to retrieve the residual stresses values. Overall, Nikiforov's numerical model tended to under-predict the residual stresses compared to the experimental values which may be a consequence of using constant thermal material properties rather than temperature dependant ones.

Fu et al. [15] also omitted the friction phases and computed a coupled thermo-mechanical analysis on a 3D model in three steps. An initial temperature field using a Gaussian distribution, representing the equilibrium temperature field was mapped onto the model, assuming a stress-free state. During the first step, the model was clamped and a forging pressure was applied for 10 s then released. The model cooled for 100 s without forging pressure (second step) and finally during third step, the model was brought to room temperature before releasing the clamp to predict the final residual stress field. Fu et al. [15] replicated numerically the LFW geometry used by Frankel et al. [29] and compared his residual stress predictions against Frankel's experiments. Results from his numerical model tend to under-predict the peak residual stress as well as predicting noticeably larger bands of tensile residual stress compared to those recorded by Frankel et al. [29]. These differences could have been enhanced by assuming a stress-free state when mapping the Gaussian distribution, neglecting the effect of the thermal expansion on the stress field.

Turner et al. [14] drew several important conclusions from his numerical analysis work. Firstly, he noticed that stresses created by the oscillations tend to disappear once the oscillations have ceased, implying that oscillations have a minimal impact on the stress field during welding. Secondly, the magnitude of the stresses developed during welding are significantly lower than those arising during cooling. Consequently, Turner concluded that the residual stress field is primarily driven by the cooling of the part after welding. The peak residual stresses recorded by Nikiforov et al. [28] was 330 MPa which was noticeably lower than those predicted by Turner et al. [14] (900 MPa) and Fu et al. [15] (500 MPa). The variance may be explained by the use of different welding conditions which are not disclosed by the authors, different part dimensions and the different material properties. Also the equilibrium temperature distributions used by Nikiforov and Fu were not validated experimentally unlike Turner who validated the temperature histories predicted by his model against thermocouples [5]. Turner et al. [14] varied the applied pressure and studied its effect on the residual stress field. A large increase of applied pressure resulted in a small decrease of the residual stress magnitude, bringing Turner et al. [14] to the conclusion that the applied pressure has only a minimal influence on the residual stress field. Similarly, Nikiforov et al. [28] and Fu et al. [15] recorded a decrease of the residual stress magnitude with large increases in the applied pressure. Fu et al. [15] conducted a study where he varied the temperature distribution while maintaining the peak temperature constant. Increasing the temperature gradient of the profile increased the residual stresses.

The primary purpose of this paper is to present a novel modelling approach, that predicts the residual stresses in a 3D structure while accounting for all the welding phases of the process and bypassing the modelling of the oscillations. The effects of rubbing velocity, burn-off rate, applied force and oscillation direction on the residual stress field are investigated.

2. Methodology

2.1. Experiments

2.1.1. Linear friction welding

Workpieces with dimensions 60 × 40 × 20 mm (see Fig. 1a) were linear friction welded at TWI Cambridge using the Thompson E20 machine for the five welding conditions presented in Table 1. The Ti-6Al-4V parent material had a bimodal microstructure and oscillations occurred in the *x* direction apart from weld 5 where it was in the *z* direction. For each weld, oscillator position, in-plane force, burn-off and applied force were monitored using high-speed data acquisition.

2.1.2. Contour method

Four contour method measurements were performed at Coventry University on selected welds made at TWI, i.e. welds 1–4 in Table 1, to measure the residual stress in the *x* direction. The welds were cut at mid-width on a Fanuc Robocut α-C600i wire electric discharge machine. A 0.25 mm diameter brass wire was used. The sample was rigidly and symmetrically clamped on the machine table. The wire electric discharge machining (WEDM) cutting parameters were tested and adjusted on an identical linear friction welded sample. All the EDM cuts were conducted along the plane P3, however two cutting directions were used and are presented in Fig. 2. Low power cutting parameters were used to conduct the cuts for the welds 1, 2 and 3. The settings were adjusted to get the best possible surface finish as well as little cutting artefacts. A self-equilibrium cutting strategy was used for weld 4 and involved cutting the material simultaneously through the tensile and compressive stress regions [30], i.e. it was cut across the plane P3 with the wire orientated along the *y* axis. Using a self-equilibrium cutting strategy, the authors hoped to minimise cutting-induced plasticity. This was not the case for the other welds where the cut passed sequentially from a compressive to a tensile stress region and finally to a second tensile region. The self-equilibrium cut was possible with high power settings, however surface roughness increases with high power parameters, potentially resulting in an under-estimation of the tensile residual stress in the weld. The WEDM cut progressed smoothly with a little variation in the cutting speed and without wire breakage.

The surface displacement profile of both cut halves of the sample was measured with a Zeiss Contura G2 coordinate measuring machine (CMM). A 3 mm diameter touch probe was used and the individual point spacing was set as 0.5 mm in both directions. The surface displacement data of the both cut halves of the sample was analysed for data aligning, cleaning, flattening and smoothing using the Matlab analysis routines according to Johnson 2008 [31]. The data smoothing was performed with a cubic spline of knot spacing 5.5 mm in both directions of the cutting plane (*y*, *z*).

A finite element (FE) model of one cut half of the sample was built and its mesh was generated from eight-node linear brick elements with reduced integration and hourglass control of type C3D8R using the ABAQUS software. The mesh size was set uniform along the sample thickness (i.e. 0.5 mm) and non-uniform along the length with 0.1 mm at the weld interface and coarsening to 2 mm. Finally a linear elastic FE analysis was performed using the measured displacement field as the input to get the stress results using a Young's modulus of 117 GPa and Poisson's ratio of 0.33.

Table 1
Welding parameters.

Weld	Freq. (Hz)	Amp. (mm)	Applied pressure (MPa)	Burn-off (mm)	Rubbing velocity (mm/s)	Interface dimension in oscillation direction
1	20	1.5	90	3	120	40 mm
2	30	2	90	3	240	40 mm
3	50	2.7	40	3	540	40 mm
4	50	2.7	90	3	540	40 mm
5	50	2.7	90	3	540	20 mm

2.1.3. Neutron diffraction

Neutron diffraction experiments on weld 1 were conducted at the ISIS facility of the Rutherford Appleton Laboratory in the UK. To reduce the path length of the neutrons within the material and improve the quality of the signal measured as well as reducing measurement times, the LFW was EDM cut through the thickness to achieve dimensions of 120 × 40 × 8 mm (originally 120 × 40 × 20 mm). A sample of 120 × 6 × 5 mm which included the weld joint was also EDM cut from the LFW weld to measure the stress-free lattice parameters. The dimensions 6 mm and 5 mm assured a stress free state in the *x* and *z* directions while residual stresses in the *y* direction have to balance along the plane P2 (see Fig. 1a) with the reduced area of 6 mm × 5 mm. Therefore, no stress is expected in the *y* direction.

The neutron diffractometer ENGIN-X was used to measure the elastic strains located in the weld at several positions. ENGIN-X is a time of flight (TOF) diffractometer using a neutron spallation source. Neutrons with different wavelengths are produced allowing multiple crystallographic planes to be measured at once at a fixed angle. Since two measurements are made simultaneously using the two detector banks positioned at a Bragg's angle of ±90° (Fig. 3), the LFW had to be repositioned once to measure the third direction. Consequently, the

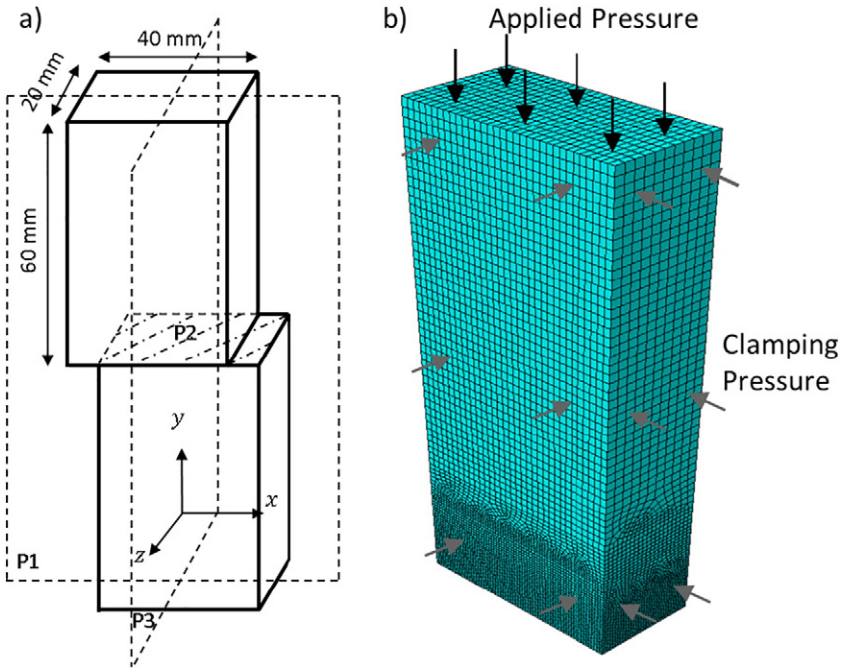

Fig. 1. a) Workpiece dimensions, axes and planes of symmetry and b) FE model representing an eighth of the real workpiece.

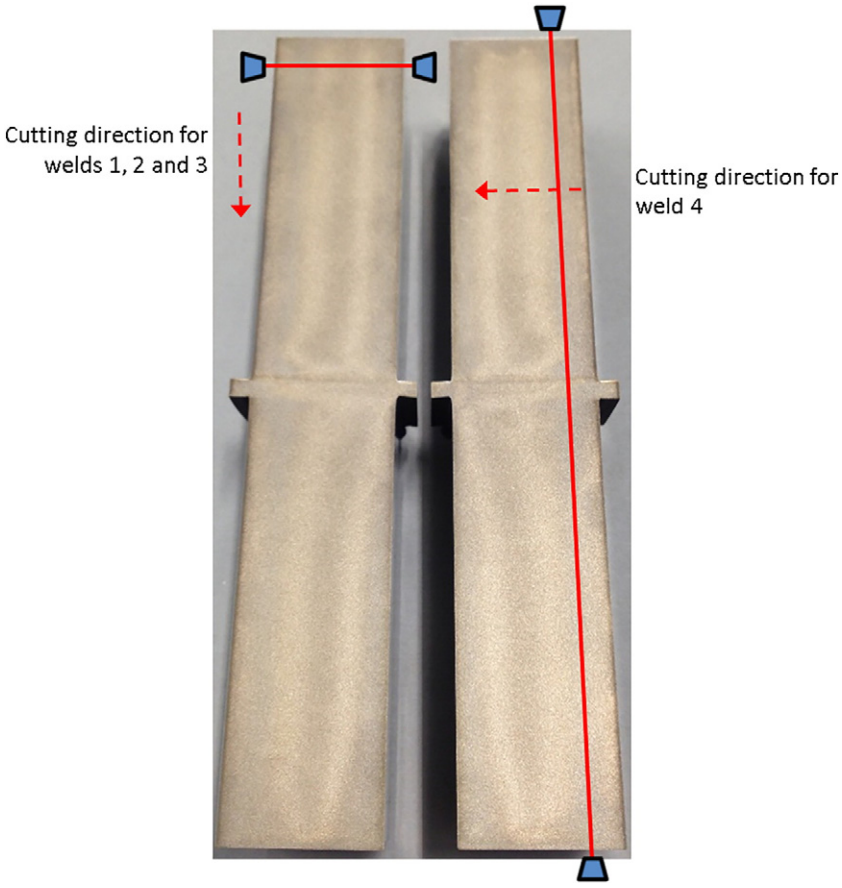

Fig. 2. EDM cut directions for the welds 1, 2, 3 and 4.

elastic strains in the z direction were measured twice allowing the repeatability of the measurements to be determined. Cuboid gauge volumes, defined by the slit dimensions and the position of the bank collimators, of $3 \times 2 \times 3$ mm were used for measuring the x and z directions and $4 \times 2 \times 3$ mm for the y and z directions. Five positions were measured in total with the first position being at the weld interface with the next three measurements being 1 mm apart and the final one 2 mm apart. Due to the limited time available at the ISIS facility, elastic strains on only one side of the weld interface were measured; however results from the literature have shown that residual stresses distributed within Ti-6Al-4V LFW are approximately symmetrical around the weld interface [27,29,32,33]. Stress-free lattice parameters were measured for each position from the stress-free specimen. Finally assuming isotropic elastic properties, Hooke's law was used to calculate the residual stresses σ_{ii} from the elastic strains ε_{ii} as follows:

$$\sigma_{ii} = \frac{E}{(1+\nu)(1-2\nu)}\left[(1-\nu)\varepsilon_{ii} + \nu\left(\varepsilon_{jj}+\varepsilon_{kk}\right)\right], \quad i,j,k \in x,y,z \tag{1}$$

where E is the Young's modulus and ν the Poisson's ratio.

The quality of the diffraction peaks was more consistent for the crystallographic plane $\{10\bar{1}1\}$ and fitting errors were minimal. Consequently, lattice distances from this plane were used to calculate elastic strains and subsequently residual stresses using a Young's modulus of 98 GPa [34] specific to this crystallographic plane $\{10\bar{1}1\}$ and a Poisson's ratio of 0.33. This Young's modulus value was only used for the neutron diffraction measurements and a temperature dependant isotropic value was used for the numerical simulations. Calculated error bars display fitting errors for the measured diffraction peaks, correctly propagated through the calculations of residual stresses.

A comparison between residual stress measured using neutron diffraction and those predicted numerically is provided in the results section. To numerically account for the EDM cut, an equivalent amount of material was removed from the model allowing the redistribution of the residual stress field. Apart from this comparison, the EDM cut was not considered within the numerical models.

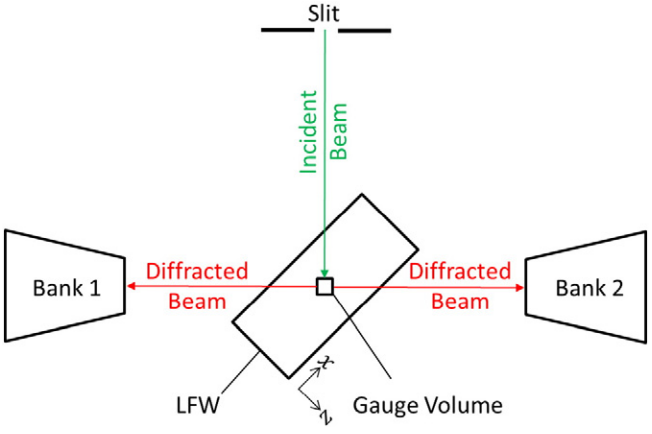

Fig. 3. Experimental set-up used with ENGIN-X diffractometer.

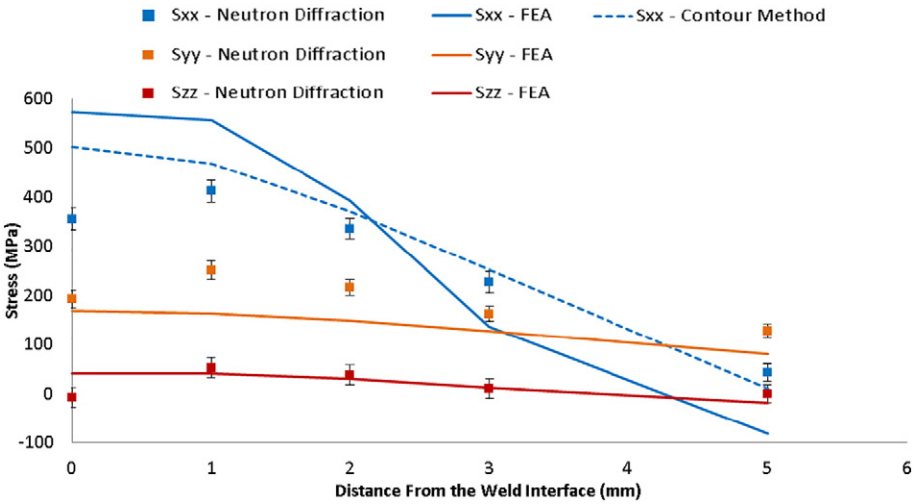

Fig. 4. Comparison of residual stresses in weld 1, measured by neutron diffraction (after EDM cut to reduce the neutron path length), contour method and predicted numerically.

2.2. Modelling approach

2.2.1. Mesh and material properties

As shown in Fig. 1a, the real workpieces are 120 × 40 × 20 mm. Since the deformation and heat flow are approximately symmetric around the planes (P1), (P2) and (P3) [11,12,19], only an eighth of the geometry was included. Therefore, a workpiece measuring 60 × 20 × 10 mm was modelled using the FEA software ABAQUS. A mesh composed of the C3D8R brick elements was used. A mesh size of 0.3 mm was used at the weld interface and its vicinity which then coarsened to 1 mm.

Temperature dependant Ti-6Al-4V material properties were used for the models. Flow stress data for temperatures less than and equal to 700 °C are taken from Chen et al. [35] at a quasi-static strain rate. From 800 °C and beyond, flow stress data from Guo et al. [36] are used; the material exhibits a drop in strength and a perfectly plastic behaviour [5]. An annealing temperature of 800 °C is defined in ABAQUS to simulate the relaxation of the accumulated stresses and strains above this temperature. Above 800 °C, Ti-6Al-4V has a reduced strength due to the high temperature experienced and becomes a single phase material when reaching the beta-transus temperature at approximately 1000 °C [37,38] where its strength significantly reduces. Above 800 °C, Ti-6Al-

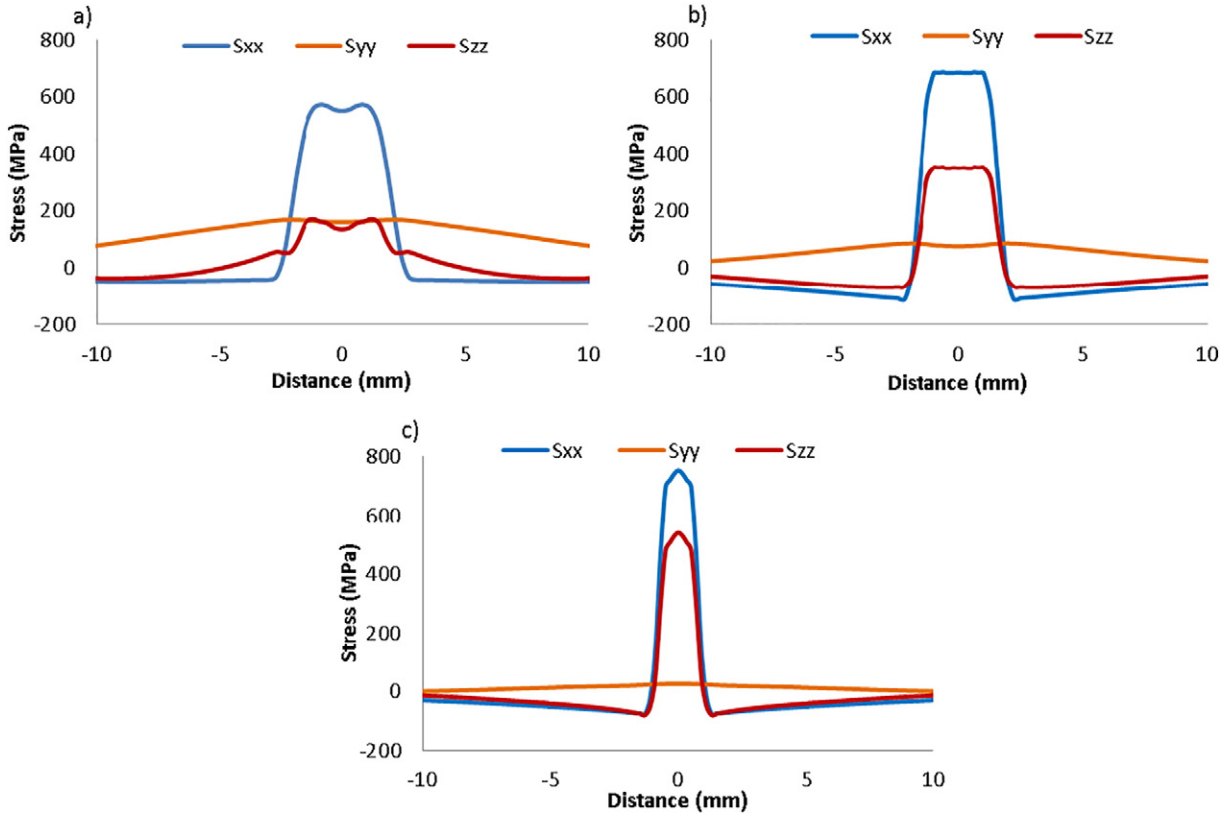

Fig. 5. Residual stress distributions in the three directions of space predicted numerically for: a) weld 1, b) weld 2 and c) weld 4.

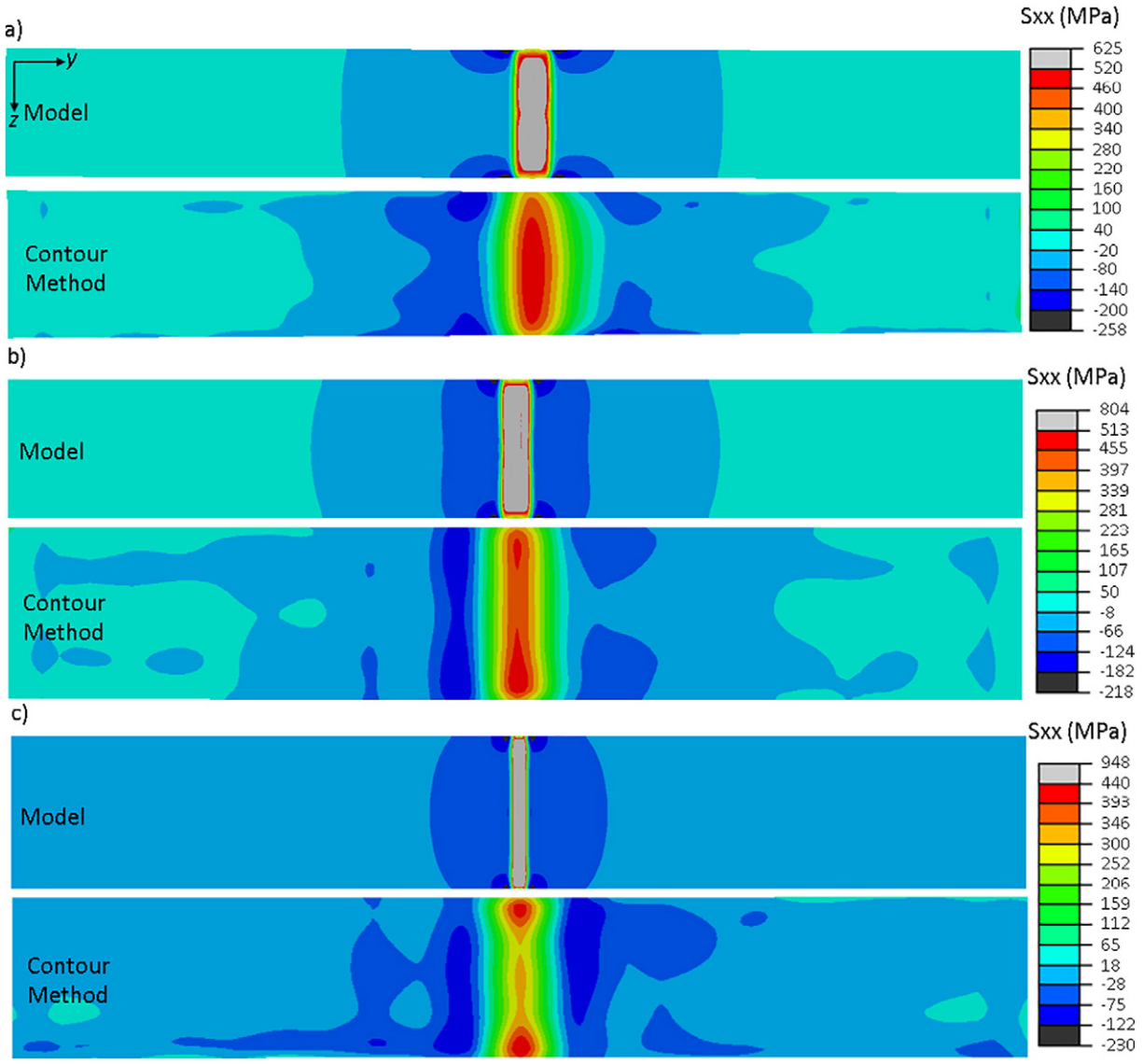

Fig. 6. Residual stress contour plots in the x direction predicted numerically and obtained by contour method: a) weld 1, b) weld 2 and c) weld 4.

4V also experiences dynamic recrystallization due to the deformation and high temperature [37,39]. Young's modulus was taken from Turner et al. [14] while thermal expansion coefficient values are from Boyer et al. [40].

2.2.2. Thermal modelling

To account for the heat generation without modelling the oscillations, an average heat flux per phase was calculated from the monitored data, obtained during welding. The heat flux was applied on the weld interface and during the phase 3, rows of elements were removed iteratively at a pace matching the experimental burn-off rate to simulate the axial shortening. The thermal modelling approach was validated against thermocouples for various welding conditions. For full details, the reader is referred to reference 41.

2.2.3. Loading, boundary conditions and modelling of the burn-off

To account for the effect of the heat on the stress field, the temperature history previously predicted using a thermal model is mapped on the mechanical model. An extra cooling step is added to bring the model to room temperature. The applied force (expressed as a pressure in Table 1) and the clamping force are both applied as pressures on the model. The clamping force represents the force applied by the clamping tool on the sides of the workpiece (Fig. 1b) and is equal to the applied force, as for the experiments. The clamping force is not applied to a band 6.6 mm from the interface as is the case with the experiments. The applied force is applied on the top surface of the workpiece. Applied force and clamping force are applied during the welding phases and for the first 15 s of cooling before being released. Three symmetry boundary conditions are applied to the model to account for the planes of symmetry P1, P2 and P3. The burn-off is accounted in the same way as in the thermal model, i.e. by sequentially removing rows of elements (see reference 41). Finally, it is worth noting that the flash creation is not simulated. The flash is located at the edges of the weld and therefore the authors believe that it is not likely to affect the residual stresses located in the centre which are of interest in this study. Turner et al. [14] modelled the flash and little or no residual stress developed in its vicinity. Ultimately, the flash was removed for the neutron diffraction and contour method measurements against which the model is compared. This modelling approach reduces the calculation time for 3D models from approximately 4 weeks [12] to 15 h.

The influence of the rubbing velocity was studied in the result section by comparing welds 1, 2 and 4. The effect of the applied force is

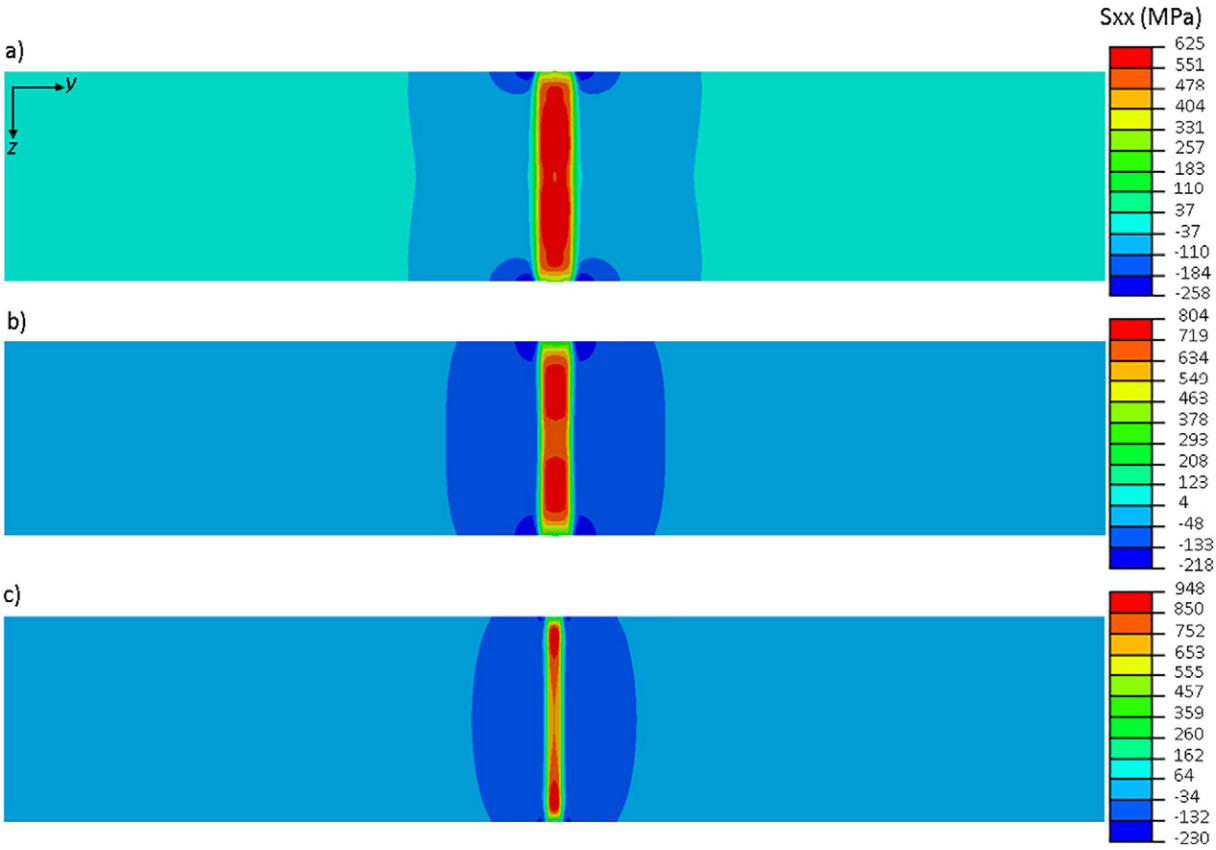

Fig. 7. Contour plots of numerically predicted residual stress in the x direction: a) weld 1, b) weld 2 and c) weld 4.

examined using welds 3 and 4, while the oscillation direction is studied using welds 4 and 5. Stress and temperature profile plots were extracted at mid-thickness of the weld in the plane P1.

3. Results and discussion

3.1. Comparison of residual stresses predicted numerically against neutron diffraction and contour method measurements

Fig. 4 presents residual stresses within weld 1, in the three directions of space calculated from the lattice parameters along with those measured using the contour method and predicted numerically after accounting for the EDM cut (model dimensions were 120 × 40 × 8 mm). Residual stresses from the contour method were predicted for the full thickness LFW. The FEA model only recorded a small variation in the residual stress magnitudes (25 MPa at the weld interface) when accounting for the EDM cut. Therefore, contour method predictions from the full thickness weld can be compared with the neutron diffraction and FEA results. Residual stresses resulting from the model and contour method were averaged over similar gauge volumes to those used for neutron diffraction to facilitate the comparison. Tensile residual stresses are located in the directions *x* and *y* while the *z* direction is virtually stress-free. As previously mentioned, the original LFW was EDM cut to reduce the neutron path length. As a consequence, the weld interface dimension in the *z* direction was reduced to 8 mm compared to the original 20 mm. Fig. 4 shows that a plane stress condition is reached in the *z* direction with a sample thickness of 8 mm. In agreement with the literature, lower tensile residual stresses are expected in the direction of the applied pressure (y axis) compared to the longest direction of the weld interface (*x* axis). Interestingly a decrease in the residual stress magnitude is recorded at the weld interface compared to the gauge volume positioned 1 mm away. A similar pattern is shown by Dewald et al.'s [33] neutron diffraction measurements. Positioning the gauge volume at the weld interface is a difficult task and combined with the effect of fitting errors are believed to be at the origin of the trend observed.

Overall, neutron diffraction, contour method and modelling predictions are in reasonable agreement. The plane stress condition in the *z* direction as a result of the EDM cut is captured by both neutron diffraction and model values. Modelling results tend to predict a higher peak of residual stress magnitude and a steeper distribution. This could be a result of the lack of accuracy of the material properties used. The full effect of the work hardening, dynamic recrystallization occurring at the interface and rapid cooling of the weld is not accounted for. Microstructural modelling capability could improve the accuracy of numerical predictions [42]. Inaccuracies introduced by the EDM cuts are discussed in the following section.

3.2. Influence of the rubbing velocity

Residual stress distributions across the interface, predicted numerically, in the three directions of space for three welding conditions, weld 1, 2 and 4 (see Table 1) are presented in Fig. 5. In each case, a band of tensile residual stress can be observed at the weld interface which becomes compressive further away and then zero at the edge of the part. This stress distribution arises as a result of the thermal contraction of the band of hot material at the weld interface while being constrained by the surrounding cold material. It is worth noticing that the highest residual stress magnitude is always located in the x direction which represents both the oscillation direction and the longest direction of the weld interface. The second highest magnitude is usually found in the second direction of the weld interface *z* while the magnitude in the direction of the applied force *y* is lower. In the case of weld 1, similar

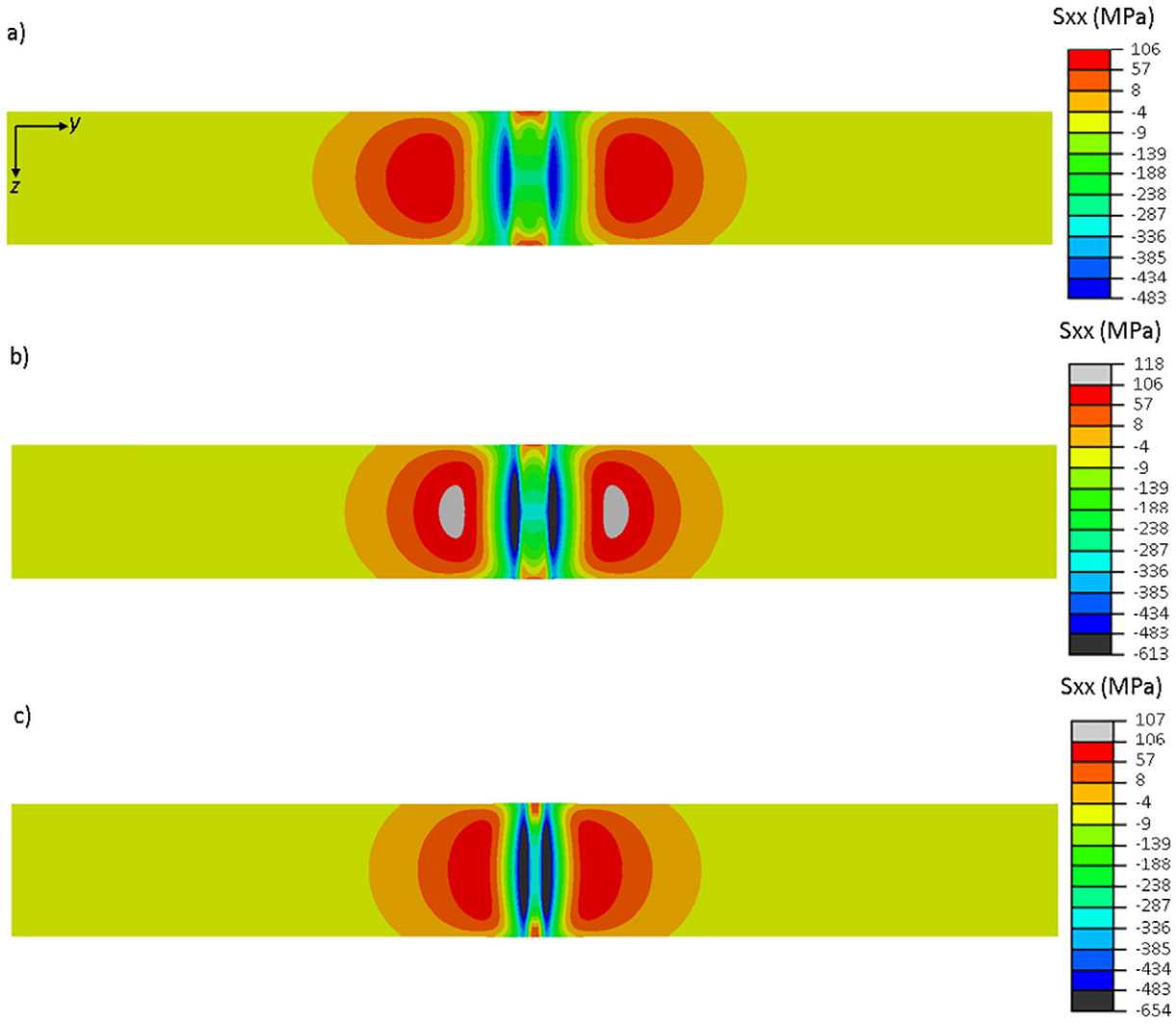

Fig. 8. Contour plots of numerically predicted equilibrium stress fields in the x direction: a) weld 1, b) weld 2 and c) weld 4.

residual stress peak magnitudes are obtained in the *y* and *z* directions and is believed to be a result of the combination of shallow thermal gradient and high applied pressure.

Contour plots of residual stress in the *x* direction obtained by numerical analysis and the contour method for the three welding conditions are displayed in Fig. 6. Residual stress distributions are coherent

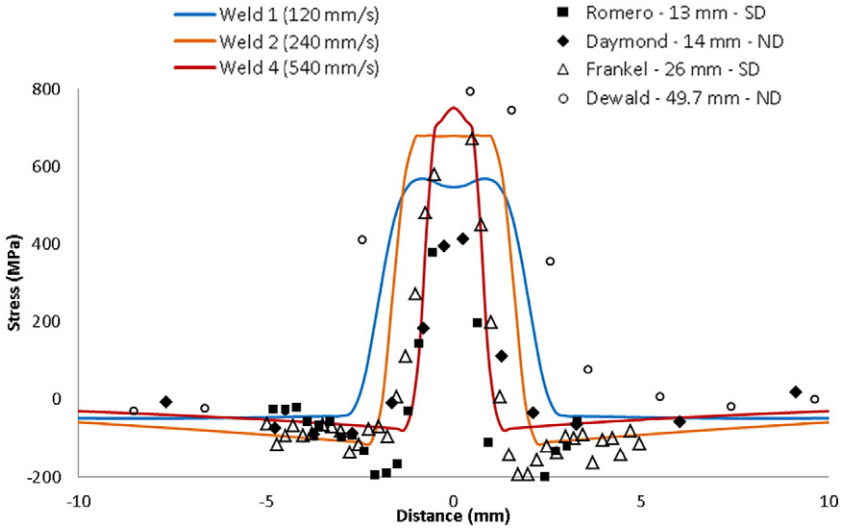

Fig. 9. Comparison of numerically predicted residual stress in the x direction and data from Romero et al. [27], Daymond et al. [32], Frankel et al. [29] and Dewald et al. [33] measured in the longest direction of the weld interface (indicated by their respective length) within Ti-6Al-4V LFW with different techniques (ND: neutron diffraction, SD: synchrotron x-ray diffraction).

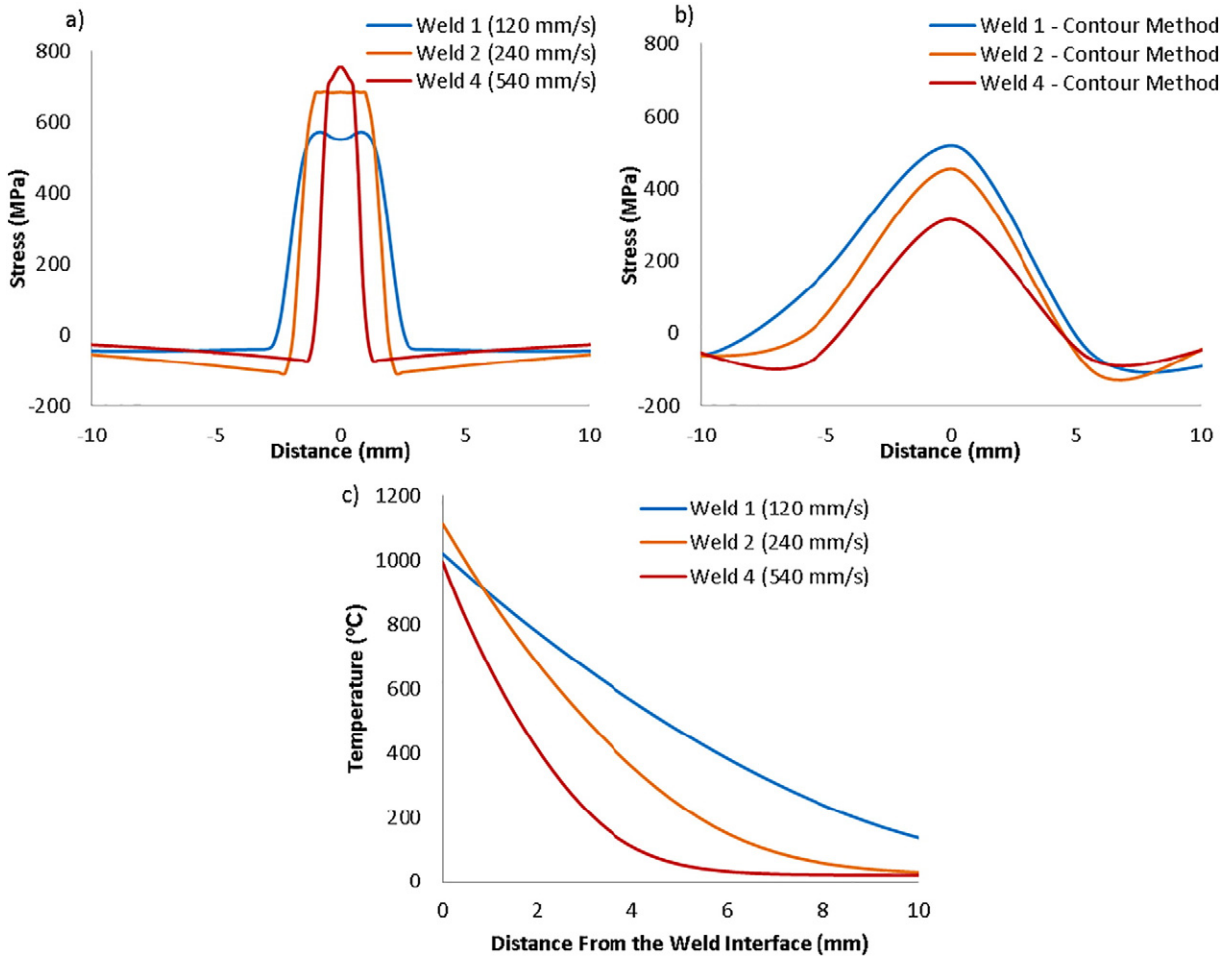

Fig. 10. Residual stresses in the *x* direction (40 mm length of the interface) obtained by a) FEA, b) contour method and c) equilibrium temperature distributions.

between numerical model and contour method. However, the contour plots clearly show that higher residual stress magnitudes and smaller band of tensile residual stress are numerically predicted. Although the EDM cut performed for the purpose of the contour method is supposedly purely elastic, cutting-induced plasticity could have been created [43,44] altering the original residual stress distribution and it is difficult to control. Plastic deformations are more likely to get created where residual stresses have high magnitudes, however owing to the localised stress concentration at the cutting front, plastic strains can also be induced in the far-field residual stress [43]. Furthermore, the contour method is known to smooth out features associated with high stress gradients as a result of the filtering process used to eliminate surface roughness effects [33]. As a consequence, the contour method tends to under-predict the peak of residual stress and creates a wider distribution [29,44]. As an additional way to assess the validity of the numerically predicted residual stress distributions, a comparison with experimental measurements from the literature [27,29,32,33] performed on Ti-6Al-4V LFW is provided Fig. 9. Those experimental measurements display a good match (residual stress magnitudes and distributions) with the numerical predictions, building confidence in this modelling approach.

Fig. 7 shows the same numerical results as Fig. 6, however the original scale was kept to visualise the positions of the residual stress peaks.

Table 2
Slope of the equilibrium temperature distribution for different weld conditions.

Weld	1	2	4
Slope (°C/mm)	−127	−231	−330

Interestingly, both contour method and numerical model predict homogenous residual stress intensity over the weld interface for weld 1 condition while for weld 2 and weld 4 the areas of highest intensity are located closer the edges with a reduction at the centre. Similar residual stress distributions were reported by Turner et al. [14] but were not discussed. To understand these distributions, it is necessary to look at the respective equilibrium stress fields, when the process reaches a quasi-steady state during phase 3, displayed in Fig. 8. The equilibrium stress field can be divided into three areas: the centre with low magnitude stresses because of the loss of strength of Ti-6Al-4V at high temperature; further away there is an area of highly compressive stresses where reduced temperature occurs, this area expands but is constrained by the surrounding cold material which puts it into compression and finally in the far field, an area of tensile stresses to balance the stress field in the workpiece. Owing to shallower temperature gradient (see Fig. 10 c) in weld 1, lower magnitude compressive stress developed further away from the interface compared to weld 2 and weld 4, see Fig. 8 a, b and c. As a consequence, the equilibrium stress field at the weld interface is homogenous resulting in a homogenous residual stress field. However, in weld 2 and weld 4 highly compressive areas are located closer to the weld interface due to their steeper temperature gradients which affect the stress field at the interface and result in higher compressive stresses at the centre of the weld compared to the edges, explaining the residual stress distributions observed in Fig. 7.

Residual stress distributions in the *x* direction extracted at mid-thickness from numerical models (Fig. 10 a) and contour method (Fig. 10 b) are plotted for comparison. Numerically, an increase in the rubbing velocity resulted in an increase in the peak of residual stress magnitude and a decrease of the size of the band of tensile residual

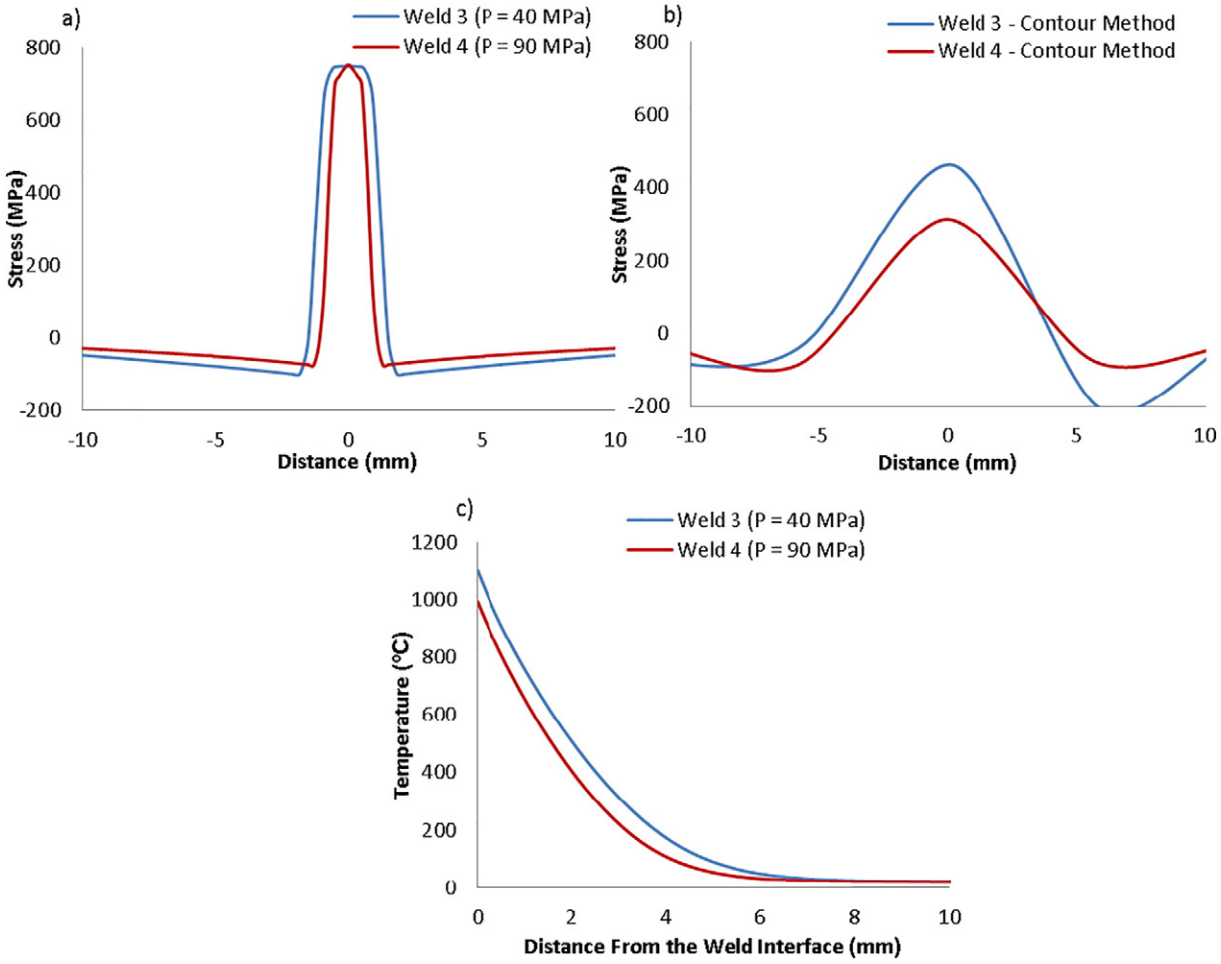

Fig. 11. Residual stresses in the *x* direction (40 mm length of the interface) obtained by a) FEA, b) contour method and c) equilibrium temperature distributions.

stress. Although the increase in magnitude is not captured by the contour method measurements, the trend of the width of the band of tensile residual stress is, as shown in Fig. 10 b. Contour method predictions of the magnitude of residual stress also contradict the trends observed by Fu et al. [15].

The effect of the rubbing velocity can be correlated with equilibrium thermal profiles obtained. Slopes of the equilibrium temperature profiles (shown in Fig. 10 c) were approximated from slope values of straight lines passing through the residual stresses predicted between 0 mm and 1 mm and are presented in Table 2. Weld 1 ($v_{rubbing} = 120$ mm/s) and weld 4 ($v_{rubbing} = 540$ mm/s) have a similar weld interface temperature (see Fig. 10 c) however weld 4 has a significantly steeper thermal gradient, as shown in Table 2. As a result, the plastic strain mismatch was enhanced and increased the peak of residual stress magnitude as well as creating a narrower band of tensile residual stress compared to a shallow thermal gradient. On the other hand, weld 4 displays a significant cooler weld interface temperature with a steeper thermal gradient than weld 2 ($v_{rubbing} = 240$ mm/s). Despite having a higher weld interface temperature, weld 2 developed a lower residual stress peak, implying that the residual stress peak magnitude is primarily driven by the thermal gradient. A larger band of tensile residual is observed for weld 2 since more heat has conducted into the workpieces due to the higher temperature and the shallower thermal gradient. As a result, more material experienced thermal contraction during the cooling.

Table 3
Slope of the equilibrium temperature distribution for different weld conditions.

Weld	3	4
Slope (°C/mm)	−329	−330

3.3. Influence of the applied force

Using an applied pressure of 90 MPa instead of 40 MPa, left the peak of residual stress magnitude unchanged and created a smaller band of tensile residual stress, as presented in Fig. 11 a. The reduction in the size of the band of tensile residual stress was also captured by the contour method, see Fig. 11 b. Similar to the previous section, higher

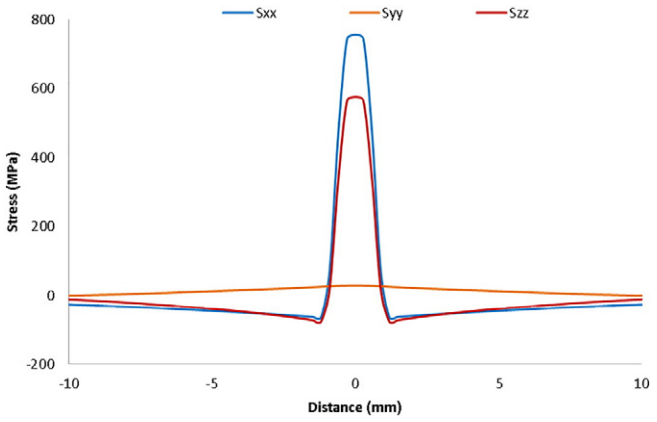

Fig. 12. Residual stress distributions in the three directions of space predicted numerically for weld 5.

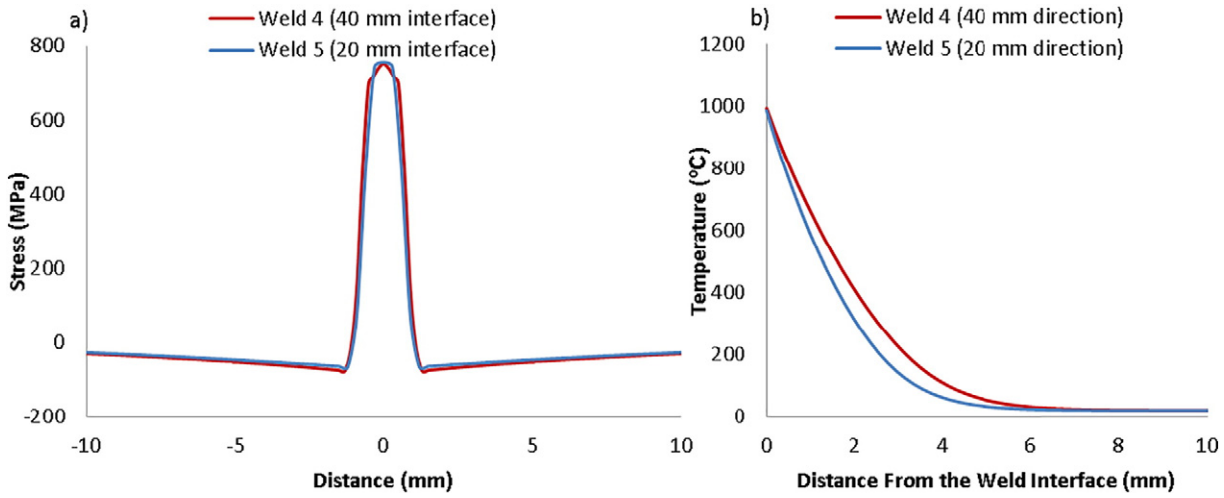

Fig. 13. a) Residual stress in the *x* direction of welds 4 and 5 and b) equilibrium temperature distribution across the weld of welds 4 and 5.

residual stress magnitude and smaller band of tensile residual stress are numerically predicted compared to those measured using contour method.

Fig. 11 a results are consistent with those observed by Turner et al. [14] and Frankel et al. [29]. Using a higher applied pressure caused the peak temperature to reduce (see Fig. 11 c) and the thermal gradient was similar, as displayed in Table 3. As a result of having a similar thermal gradient, a similar peak of residual stress is created for both welding conditions. Furthermore, due to weld 4's lower interface temperature, less material experienced thermal contraction resulting in a smaller band of tensile residual stress. These findings show that similar results to the fully-coupled numerical model developed by Turner et al. [14] are achieved using this sequentially-coupled modelling approach.

3.4. Influence of the oscillation direction

The residual stress distributions in the three directions of space predicted numerically for weld 5 are presented in Fig. 12. Despite oscillating in the 20 mm weld interface direction (i.e. *z* direction) rather than the 40 mm (i.e. *x* direction), the highest residual stresses are located in the *x* direction. It can be concluded that the highest residual stress are developed in the longest direction of the weld interface irrespective of the oscillation direction.

The residual stress distributions in the *x* direction obtained for welds 4 and 5 and their associated equilibrium temperature profiles are displayed in Fig. 13. Oscillating in the 40 mm weld interface direction with weld 4 rather than the 20 mm direction with weld 5 resulted in an equivalent peak temperature at the end of phase 3 (see Fig. 13 b) and a steeper thermal gradient for weld 5, see Table 4. Despite a higher equilibrium temperature slope value, the residual stress profile created by weld 5 is similar to weld 4. Therefore, the peak of residual stress does not increase proportionally with the magnitude of the thermal gradient in this case; more work is necessary to fully understand the development of residual stresses and their interactions with their associated equilibrium temperature profile.

Table 4
Slope of the equilibrium temperature distribution for different weld conditions.

Weld	4	5
Slope (°C/mm)	−330	−389

4. Conclusions

The key findings from this work are:

1. A good agreement was found between residual stresses numerically predicted for weld 1 and those measured using neutron diffraction and the contour method. It is worth noting that weld 1 exhibited the lowest peak and the widest residual stress distribution, making it the easiest welding condition to be experimentally measured.
2. Numerical models predicted higher peaks and narrower distributions of residual stress compared to the contour method for the other welding conditions. These discrepancies are believed to have been enhanced by cutting-induced plasticity and increased surface roughness owing to the EDM cut. Numerically predicted residual stresses were found to be in good agreement with experimental measurements of LFW available in the literature, both in terms of magnitude and distribution.
3. Increasing the rubbing velocity resulted in an increase of the peak of residual stress for the model and a narrower band of tensile residual stress. The trend of the effect of the rubbing velocity on the residual stress distribution was also captured by the contour method. An increase in the applied pressure did not change the peak of residual stress while narrowing the residual stress distribution; while oscillating in the 20 mm direction of the interface rather than the 40 mm direction was found to have no influence on the residual stress profile.
4. A strong correlation between the equilibrium temperature distribution and the residual stress field has been established. The residual stress distribution was shown to be dominated by the thermal gradient of the equilibrium temperature field. Steep thermal gradients lead to high peak values of residual stress while narrowing the band of tensile residual stress. As a secondary influence, high weld interface temperature tends to enlarge the band of tensile residual stress as a result of conducting more heat from the weld interface.
5. This approach provides a computationally efficient technique to study the residual stress development within large realistic engineering workpieces where a 2D assumption for the modelling approach cannot be assumed.

Acknowledgements

The authors would like to thank the Honeywell Aerospace and Cranfield University for funding the research presented in that paper.

Also, the help provided by Dr Supriyo Ganguly and Jan R. Hönnige (Cranfield University) in conducting the neutron diffraction experiments was greatly appreciated. We are thankful to Steve Damms at The Institute for Advanced Manufacturing and Engineering for the WEDM.

References

[1] B.V.R.R.A. Kumar, Review on blisk technology, Int. J. Innov. Res. Sci. Eng. Technol. 2 (2013) 1353–1358.
[2] P. Wanjara, M. Jahazi, Linear friction welding of Ti-6Al-4V: processing, microstructure, and mechanical-property inter-relationships, Metall. Mater. Trans. A 36 (2005) 2149–2164.
[3] W. Li, H. Wu, T. Ma, C. Yang, Z. Chen, Influence of parent metal microstructure and post-weld heat treatment on microstructure and mechanical properties of linear friction welded Ti-6Al-4V joint, Adv. Eng. Mater. 14 (2012) 312–318.
[4] U.U. Ofem, P.A. Colegrove, A. Addison, M.J. Russell, Energy and force analysis of linear friction welds in medium carbon steel, Sci. Technol. Weld. Join. 15 (2010) 479–485.
[5] R. Turner, J.-C. Gebelin, R.M. Ward, R.C. Reed, Linear friction welding of Ti–6Al–4V: modelling and validation, Acta Mater. 59 (2011) 3792–3803.
[6] A.R. McAndrew, P.A. Colegrove, A.C. Addison, B.C.D. Flipo, M.J. Russell, Energy and force analysis of Ti-6Al-4V linear friction welds for computational modeling input and validation data, Metall. Mater. Trans. A 45 (2014) 6118–6128.
[7] L. Fratini, G. Buffa, D. Campanella, D. La Spisa, Investigations on the linear friction welding process through numerical simulations and experiments, Mater. Des. 40 (2012) 285–291.
[8] W.-Y. Li, T. Ma, J. Li, Numerical simulation of linear friction welding of titanium alloy: effects of processing parameters, Mater. Des. 31 (2010) 1497–1507.
[9] A. Vairis, M. Frost, High frequency linear friction welding of a titanium alloy, Wear 217 (1998) 117–131.
[10] F. Schroeder, R.M. Ward, R.P. Turner, A.R. Walpole, M.M. Attallah, J.-C. Gebelin, R.C. Reed, Validation of a model of linear friction welding of Ti6Al4V by considering welds of different sizes, Metall. Mater. Trans. B Process Metall. Mater. Process. Sci. 46 (2015) 2326–2331.
[11] A.R. McAndrew, P.A. Colegrove, A.C. Addison, B.C.D. Flipo, M.J. Russell, L.A. Lee, Modelling of the workpiece geometry effects on Ti–6Al–4V linear friction welds, Mater. Des. 87 (2015) 1087–1099.
[12] A.R. McAndrew, P.A. Colegrove, A.C. Addison, B.C.D. Flipo, M.J. Russell, Modelling the influence of the process inputs on the removal of surface contaminants from Ti–6Al–4V linear friction welds, Mater. Des. 66 (2015) 183–195.
[13] F. Schroeder, R.M. Ward, R.P. Turner, M.M. Attallah, J. Gebelin, R.C. Reed, Linear friction welding of titanium alloys for aeroengine applications: modelling and validation, In 9th Int. Conf. Trends Weld. Res 2012, pp. 886–892.
[14] R. Turner, R.M. Ward, R. March, R.C. Reed, The magnitude and origin of residual stress in Ti-6Al-4V linear friction welds: an investigation by validated numerical modeling, Metall. Mater. Trans. B Process Metall. Mater. Process. Sci. 43 (2012) 186–197.
[15] Y. Fu, W.-Y. Li, X.-W. Yang, T.-J. Ma, A. Vairis, The effects of forging pressure and temperature field on residual stresses in linear friction welded Ti6Al4V joints, Adv. Manuf. 4 (2016) 314–321.
[16] S.K. Kiselyeva, A.M. Yamileva, M.V. Karavaeva, Computer modelling of linear friction welding based on the joint microstructure, J. Eng. Sci. Technol. Rev. 5 (2012) 44–47.
[17] J. Sorina-Müller, M. Rettenmayr, D. Schneefeld, O. Roder, W. Fried, FEM simulation of the linear friction welding of titanium alloys, Comput. Mater. Sci. 48 (2010) 749–758.
[18] W.Y. Li, S.X. Shi, F.F. Wang, T.J. Ma, J.L. Li, D.L. Gao, A. Vairis, Heat reflux in flash and its effect on joint temperature history during linear friction welding of steel, Int. J. Therm. Sci. 67 (2013) 192–199.
[19] A. Vairis, M. Frost, Modelling the linear friction welding of titanium blocks, Mater. Sci. Eng. A 292 (2000) 8–17.
[20] A.M. Yamileva, R.K. Gazizov, A. Vairis, Computer modelling of the effect of clamping in linear friction welding, J. Eng. Mater. Technol. 8 (2015) 65–68.
[21] A.R. McAndrew, P.A. Colegrove, B.C.D. Flipo, C. Bühr, 3D modelling of Ti–6Al–4V linear friction welds, Sci. Technol. Weld. Join. 1718 (2016) 1–9.
[22] E. Ceretti, L. Fratini, C. Giardini, D. La Spisa, Numerical modelling of the linear friction welding process, Int. J. Mater. Form. 3 (2010) 1015–1018.
[23] M. Grujicic, G. Arakere, B. Pandurangan, C.-F. Yen, B.A. Cheeseman, Process modeling of Ti-6Al-4V linear friction welding (LFW), J. Mater. Eng. Perform. 21 (2012) 2011–2023.
[24] P. Zhao, L. Fu, D. Zhong, Numerical simulation of transient temperature and axial deformation during linear friction welding between TC11 and TC17 titanium alloys, Comput. Mater. Sci. 92 (2014) 325–333.
[25] W. Li, F. Wang, S. Shi, T. Ma, J. Li, A. Vairis, 3D finite element analysis of the effect of process parameters on linear friction welding of mild steel, J. Mater. Eng. Perform. 23 (2014) 4010–4018.
[26] P.J. Blau, The significance and use of the friction coefficient, Tribol. Int. 34 (2001) 585–591.
[27] J. Romero, M.M. Attallah, M. Preuss, M. Karadge, S.E. Bray, Effect of the forging pressure on the microstructure and residual stress development in Ti–6Al–4V linear friction welds, Acta Mater. 57 (2009) 5582–5592.
[28] R. Nikiforov, A. Medvedev, E. Tarasenko, A. Vairis, Numerical simulation of residual stresses in linear friction welded joints, J. Eng. Sci. Technol. Rev. 8 (2015) 157–173.
[29] P. Frankel, M. Preuss, A. Steuwer, P.J. Withers, S. Bray, Comparison of residual stresses in Ti–6Al–4V and Ti–6Al–2Sn–4Zr–2Mo linear friction welds, Mater. Sci. Technol. 25 (2009) 640–650.
[30] O. Muránsky, C.J. Hamelin, F. Hosseinzadeh, M.B. Prime, Evaluation of a self-equilibrium cutting strategy for the contour method of residual stress measurement, Int. J. Press. Vessel. Pip. (2016) 1–10.
[31] G. Johnson, Residual Stress Measurements Using the Contour Method, 2008.
[32] M.R. Daymond, N.W. Bonner, Measurement of strain in a titanium linear friction weld by neutron diffraction, Phys. B Condens. Matter 325 (2003) 130–137.
[33] DeWald, A. T., Legzdina, D., Clausen, B., Brown, D. W., Sisneros, T. A. & Hill, M. R. in (eds. Ventura, C. E., Crone, W. C. & Furlong, C.) 4, 183–189 (Springer New York, 2013).
[34] A.M. Stapleton, S.L. Raghunathan, I. Bantounas, H.J. Stone, T.C. Lindley, D. Dye, Evolution of lattice strain in Ti–6Al–4V during tensile loading at room temperature, Acta Mater. 56 (2008) 6186–6196.
[35] G. Chen, C. Ren, X. Qin, J. Li, Temperature dependent work hardening in Ti–6Al–4V alloy over large temperature and strain rate ranges: experiments and constitutive modeling, Mater. Des. 83 (2015) 598–610.
[36] Z. Guo, N. Saunders, A.P. Miodownik, Modelling high temperature flow stress curves of titanium alloys, MRS Int. Mater. Res. Conf, 2008.
[37] T. Seshacharyulu, S.C. Medeiros, W.G. Frazier, Y.V.R.K. Prasad, Hot working of commercial Ti–6Al–4V with an equiaxed α–β microstructure: materials modeling considerations, Mater. Sci. Eng. A 284 (2000) 184–194.
[38] M. Boivineau, C. Cagran, D. Doytier, V. Eyraud, M.-H. Nadal, B. Wilthan, G. Pottlacher, Thermophysical properties of solid and liquid Ti-6Al-4V (TA6V) alloy, Int. J. Thermophys. 27 (2006) 507–529.
[39] T. Seshacharyulu, S.C. Medeiros, W.G. Frazier, Y.V.R.K. Prasad, Microstructural mechanisms during hot working of commercial grade Ti–6Al–4V with lamellar starting structure, Mater. Sci. Eng. A 325 (2002) 112–125.
[40] Rodney Boyer, Gerhard Welsch, E. Collings, Materials Properties Handbook: Titanium Alloys, ASM International, 1994.
[41] C. Bühr, P.A. Colegrove, A.R. McAndrew, A computationally efficient thermal modelling approach of the linear friction welding process, J. Mater. Process. Technol. (2017)https://doi.org/10.1016/j.jmatprotec.2017.09.013.
[42] R. Turner, F. Schroeder, R.M. Ward, J.W. Brooks, The importance of materials data and modelling parameters in an FE simulation of linear friction welding, Adv. Mater. Sci. Eng. 2014 (2014) 1–8.
[43] Y.L. Sun, M.J. Roy, A.N. Vasileiou, M.C. Smith, J.A. Francis, F. Hosseinzadeh, Evaluation of errors associated with cutting-induced plasticity in residual stress measurements using the contour method, Exp. Mech. 57 (2017) 719–734.
[44] Y. Traoré, F. Hosseinzadeh, P.J. Bouchard, Plasticity in the contour method of residual stress measurement, Adv. Mater. Res. 996 (2014) 337–342.